Position-referenced microscopy for live cell culture monitoring

July A. Galeano Z.,[1] Patrick Sandoz,[1,*] Emilie Gaiffe,[2] Sophie Launay,[3] Laurent Robert,[4] Maxime Jacquot,[1] Fabienne Hirchaud,[2] Jean-Luc Prétet,[2] and Christiane Mougin[2]

[1]*Département D'Optique P.M. Duffieux, Institut FEMTO-ST, UMR CNRS 6174, Université de Franche-Comté, 16 Route de Gray, 25030 Besançon, France*
[2]*Laboratoire de Biologie Cellulaire et Moléculaire, EA3181, IFR IBCT 133, Université de Franche-Comté, CHU Jean Minjoz, F25030 Besançon, France*
[3]*IFR IBCT 133, Université de Franche-Comté, CHU Jean Minjoz, F25030 Besançon, France*
[4]*MIMENTO technological facility, Institut FEMTO-ST, UMR CNRS 6174, Université de Franche-Comté, 32 Av. de l'Observatoire, 25044 Besançon, France*
**patrick.sandoz@univ-fcomte.fr*

Abstract: Position-referenced microscopy (PRM) is based on smart sample holders that integrate a position reference pattern (PRP) in their depth, allowing the determination of the lateral coordinates with respect to the sample-holder itself. Regions of interest can thus be retrieved easily after culture dish transfers from a cell incubator to the microscope stage. Images recorded at different instants in time are superimposed in a common coordinate system with subpixel accuracy. This paper presents such smart Petri culture dishes and their use for live cell culture monitoring. The impact of the PRP on the light budget is discussed and performances are demonstrated. First results on the application of PRM to the observation of apoptotic body internalization are reported.

© 2011 Optical Society of America

OCIS codes: (170.0180) Live cell culture; (100.0100) Image processing; (120.5050) Phase measurement; (120.0120) Instrumentation, measurement, and metrology; (180.2520) Fluorescence microscopy.

References and links

1. Y. L. Wang and D. L. Taylor, *Fluorescence Microscopy of Living Cells in Culture* (Academic Press, 1989).
2. T. W. J. Gadella Jr., T. M. Jovin, and R. M. Clegg, "Fluorescence lifetime imaging microscopy (FLIM): spatial resolution of microstructures on the nanosecond time scale," Biophys. Chem. **48**, 221–239 (1993).
3. M. Rajadhyaksha, M. Grossman, D. Esterowitz, R. H. Webb, and R. R. Anderson, "In vivo confocal scanning laser microscopy of human skin: melanin provides strong contrast," J. Invest. Dermatol. **104**, 946–952 (1995).
4. J. G. Fujimoto, "Optical coherence tomography for ultrahigh resolution in vivo imaging," Nat. Biotechnol. **21**, 1361–1367 (2003).
5. B. Feldman, "Microscope slide," U.S. Patent 4,183,614 (15 January 1980).
6. P. Lin and F. Ruddle, "Photoengraving of coverslips and slides to facilitate monitoring of micromanipulated cells or chromosome spreads," Exp. Cell Res. **134**, 485–488 (1981).
7. K. M. Saleh, P. G. Toner, K. E. Carr, and H. E. Hughes, "An improved method for sequential light and scanning electron microscopy of the same cell using localising microcoverslips," J. Clin. Pathol. **35**, 576–580 (1982).
8. F. Ruddle and P. Lin, "Method for engraving a grid pattern on microscope slides and slips," U.S. Patent 4,415,405 (15 November 1983).
9. G. Dimou and T. Pang, "Process for manufacturing a cover glass with a viewing field," U.S. Patent 5,766,677 (16 June 1998).
10. L. Hause and D. Jeutter, "Mapping method for a microscope slide," U.S. Patent 5,786,130 (28 July 1998).

#140190 - $15.00 USD Received 4 Jan 2011; revised 13 Apr 2011; accepted 14 Apr 2011; published 25 Apr 2011

11. D. St-Jacques, S. Martel, and T. B. FitzGerald, "Nanoscale grid based positioning system for miniature instrumented robots," *Proceedings of IEEE Canadian Conference on Electrical and Computer Engineering* (IEEE 2003) **3** 1831–1834.
12. P. Sandoz, R. Zeggari, L. Froelhy, J. L. Prétet, and C. Mougin, "Position referencing in optical microscopy thanks to sample holders with out-of-focus encoded patterns," J. Microsc. **255**, 293–303 (2007).
13. J. A. Galeano-Zea, P. Sandoz, E. Gaiffe, J. L. Prétet, and C. Mougin, "Pseudo-periodic encryption of extended 2-D surfaces for high accurate recovery of any random zone by vision," Int. J. Optomechatron. **4**, 65–82 (2010).
14. J. W. Goodman, *Introduction to Fourier Optics* (McGraw Hill, 1996).
15. K. Matsushima, H. Schimmel, and F. Wyrowski, "Fast calculation method for optical diffraction on tilted planes by use of the angular spectrum of plane waves," J. Opt. Soc. Am. A **20**, 1755–1762 (2003).
16. A. Marian, F. Charrière, T. Colomb, F. Montfort, J. Kühn, P. Marquet, and C. Depeursinge, "On the complex three-dimensional amplitude point spread function of lenses and microscope objectives: theoretical aspects, simulations and measurements by digital holography," J. Microsc. **225**, 156-169 (2007).
17. J. A. Galeano Z., *Position referenced microscopy: microfabricated pseudo-periodic patterns for absolute positionning of specimens with sub-micrometer accuracy*, PhD dissert., Universtié de Franche-Comté (2010).
18. J. Galeano Zea, P. Sandoz, and L. Robert, "Position encryption of extended surfaces for subpixel localization of small-sized fields of observation," in *Proceedings of IEEE Conference ISOT 2009 on Intern. Symp. on Optomechatr. Tech.* (IEEE, 2009) pp. 21–27.
19. R. J. Hansman, "Characteristics of instrumentation," in *The Measurement, Instrumentation, and Sensors Handbook*, ed. by J. G. Webster (Springer-Verlag, 1999).
20. B. Fadeel and S. Orrenius, "Apoptosis: a basic biological phenomenon with wide-ranging implications in human disease," J. Int. Med. **258**, 479–517 (2005).
21. H. zur Hausen, "Papillomaviruses in the causation of human cancers: a brief historical account," Virology **384**, 260–265 (2009).
22. E. Gaiffe, M. Saunier, S. Launay, P. Oudet, J. L. Prétet, and C. Mougin, "Horizontal transfer of viral oncogenes: An alternative pathway of carcinogenesis," Presented at 25th International Papillomavirus Conference, Malmo, Sweden, 9-14 May 2009.

1. Introduction

Permanent transformation is an intrinsic characteristic of living systems. For example living organisms undergo constant remodeling during their lifetime. These modifications occurring at different scales and at different rates can be linked to physiological (metabolism, development, differentiation or multiplication) or pathological (degeneration, immortalization, transformation) mechanisms. From the point of view of microscopy imaging, in addition to expectations on image quality and definition, this particularity of living bodies sets two complementary requirements on image acquisition durations:

- Image acquisition has to be sufficiently short to avoid blurring effects due to biological mechanisms occurring within the specimen while the image is being recorded.
- Sequences of images have to be recorded over time in order to cover the biological process involved over its whole duration.

To fulfil the first point, many techniques have been developed successfully in recent decades. New techniques or apparatus become progressively reference tools in biology and medical laboratories (for instance) [1–4]. These new methods have also a direct impact on the second point since short acquisition times allow the recording of image sequences at high rate and thus the complete documentation of fast processes. However, very little work has been interested in longer time-constant processes and in the right way to manage living-specimen observations over days or weeks. Nowadays in the field of cell culture, videomicroscopy is used as a reference method. It couples a microscope with an incubation chamber ensuring cell survival by controlling temperature, humidity and CO_2 concentration. For each experiment, this equipment is monopolized during the entire protocol duration for the observation of a single culture dish. A series of sites of interest can however be observed in parallel by means of computer-controlled stages providing micrometer repeatability in lateral specimen positioning.

#140190 - $15.00 USD Received 4 Jan 2011; revised 13 Apr 2011; accepted 14 Apr 2011; published 25 Apr 2011
(C) 2011 OSA

While videomicroscopy is effective, the exclusive use of expensive equipment for a single experiment is a drawback, especially in the case of slow processes requiring long term observations. An alternative way consists in transferring cell cultures from the cell incubator to the microscope stage for every observation and then to return the specimen to the incubator until the next observation. In this way, the microscope is made available for other users. But a new problem arises: how to localize the same regions of interest every time that the specimen is returned onto the microscope stage? This problematic has been addressed in several ways during the 1980's [5–8] and then at the end of the 1990's [9,10]. All solutions are based on grids suited to partition the specimen surface in labeled sub-surfaces that can be easily identified visually by the operator. These devices allow visual recognition of regions of interest but do not provide accurate position data suitable for precise image registration. More recently, St-Jacques et al. proposed a similar approach in the field of robotics in which a sub-surface label is encoded within the actual width of the grid separations [11].

In a previous paper we introduced a position referencing principle based on a pseudo-periodic position reference pattern (PRP) [12]. The latter is suited for lateral coordinate determination of each recorded image with respect to the sample-holder itself. This principle was demonstrated to provide a high resolution and was applied to cell preparations fixed on a microscope slide. Since position is referenced to the sample holder itself, specimens are not required to remain on the microscope stage and regions of interest can be easily localized from position data. The present paper reports on advances and characterization of the method. The technique is now applied to Pétri culture dishes and actually exploited in live cell culture experiments. In section 2 we briefly recall the PRM principle and present smart Pétri culture dishes integrating a wide PRP. Section 3 reports on positioning capabilities of the developed patterns. We demonstrate improvements in image registration quality in comparison with that allowed by microstage repeatability. Finally Section 4 illustrates a biological application of the method in the frame of experiments intended to document the internalization of apoptotic bodies by human fibroblasts. The method's capabilities to comply with different microscopy modes is thus clearly demonstrated.

2. Position-referenced microscopy (PRM)

In the field of live cell culture, the PRM principle benefits from two complementary properties:

- To survive and proliferate, cells in culture have first to adhere to the culture dish surface. At a given instant in time, it is then equivalent to locate individual cells or their spatial position on the culture dish surface.
- The short depth of focus of optical microscope objectives allows some kind of vertical multiplexing of a biological image with a PRP image.

As shown in Figs. 1(a) and 1(b), the image of the cell culture is obtained as the lens is focused on the upper side of the culture dish surface. This biological image is referenced in position thanks to the recording of a second image, as shown in Figs. 1(c) and 1(d), after vertical shifting of the focusing depth in order to image the PRP. These two levels of imaging are separated by a transparent layer made of bio-compatible polymer (PDMS). The thickness of this layer; i.e. about $40\mu m$ in our case; is adjusted in order to avoid image crosstalk while maintaining an overall thickness that is compatible with the working distance of the lens. A photograph of a smart culture dish that has been developed is shown in Fig. 2. The PRP is first produced by photolithography on a glass coverslip and then covered by the transparent polymer layer. This position-referenced part is finally stuck on the bottom side of usual culture dish that has been previously pierced to minimize the final thickness of the smart culture dish obtained. The

#140190 - $15.00 USD Received 4 Jan 2011; revised 13 Apr 2011; accepted 14 Apr 2011; published 25 Apr 2011
(C) 2011 OSA

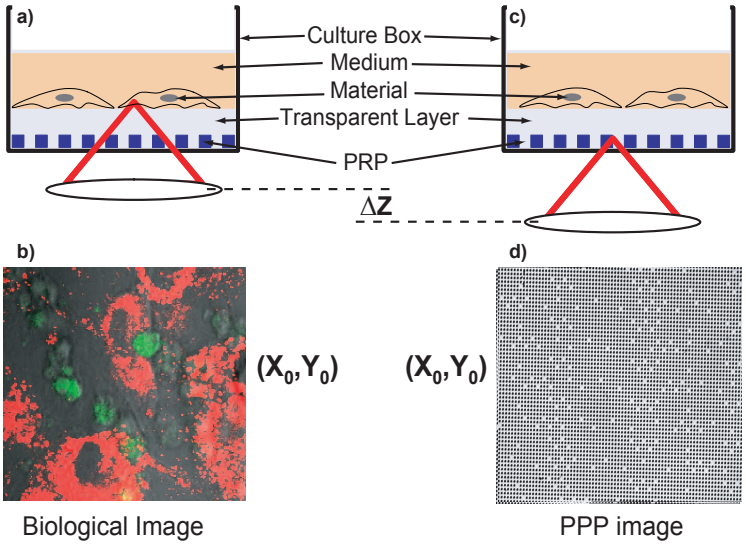

Fig. 1. PRM principle. (a) Focusing on the biological material; (b) Biological image recorded (phase contrast plus confocal fluorescence, see Section 4.2); (c) Focusing on the PRP; (d) PRP image recorded (phase contrast).

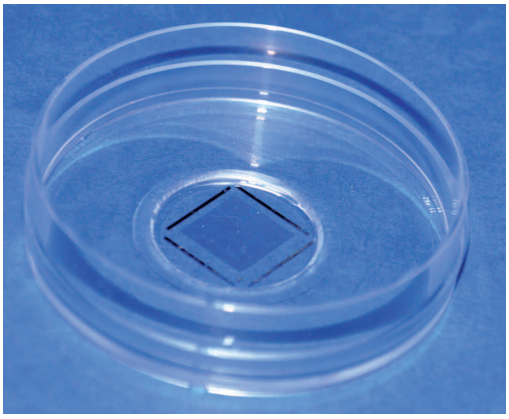

Fig. 2. Photograph of a position-referenced culture box; the patterned coverslip is stuck on the box aperture with bio-compatible polymer.

#140190 - $15.00 USD Received 4 Jan 2011; revised 13 Apr 2011; accepted 14 Apr 2011; published 25 Apr 2011
(C) 2011 OSA

encoded surface is $1\,cm^2$ wide and appears as a gray shade within black lines in Fig. 2. This spatial extension defines the size of the area available for PRM applications. The PRP conception as well as the image processing methods used for position reconstruction are described in detail elsewhere [13] and summarized in the following section. Lateral coordinate data obtained from PRP image processing are also valid for the biological image since the only displacement operated between the recording of both images is vertical. Thanks to the PRM principle, any biological image recorded is thus position-referenced with respect to the culture dish. Any position of interest can be found easily at any time; i.e. after several culture dish transfers from the microscope stage to the incubator and vice-versa. Furthermore, recorded images can be registered digitally to be displayed in a common reference system. Image superimpositions with subpixel accuracy can thus be obtained. The latter can be used for reconstructing image sequences or videos presenting the transformations of any region of interest with the same spatial accuracy as if the culture dish had been maintained static on the microscope stage during the whole protocol duration.

3. PRM performances

3.1. Basics of position encryption and reconstruction

The PRP is based on a pseudo-periodic frame of partially reflective spots on a transparent background (Fig. 1(d)) [13]. The periodic frame allows phase measurements; i.e. a fine interpolation of the elementary period of the pattern; that result in high accuracy in position measurement. The periodic frame is however made pseudo-periodic by removing a fraction of the dots in such a way to encrypt the order of each line and column of dots with respect to the top left corner of the PRP. In such a way, 2π phase ambiguities inherent to phase measurements are compensated in an absolute way through the decryption of the missing dot distribution present in each field of observation. Once a local image of the PRP is recorded, its position with respect to the PRP coordinate system is reconstructed in two steps. The first step involves linear phase processing. It allows the sharp localization of the periodic dot distribution with respect to the pixel frame of the recorded image (fine measurement) as well as the in-plane orientation of the view. The second step involves binary image processing. Its aim is to identify the distribution of the missing spots for the determination of the order of the lines and columns under view. This results in a coarse but absolute position measurement. The latter is combined with the fine but relative measurement provided by the phase processing to finally give the fine and absolute position of the zone under view.

3.2. Effect of PRP on light budget

If an inverted microscope is used as described in Fig. 1, the PRP has to be crossed twice in the formation of the biological material image. This section considers the impact of the PRP on the imaging system performance and on the final light budget of PRM. From the point of view of optical wave propagation, the problem consists in determining the disturbances of the point spread function (PSF) observed in the focusing plane that are due to the presence of the PRP. Figure 3(a) represents the intensity distribution of the converging wave in the plane just behind the PRP. In this plane, the optical wave is given by the product of the PRP transparency by usual spherical wave, here with a gaussian intensity distribution. The phase change due to the PRP comes from the coverslip thickness and can be considered to be uniform. The converging wave has thus usual spherical phase distribution associated with an intensity distribution as in Fig. 3(a). The propagation of the altered spherical wave up to the focusing plane has been calculated by using the angular spectrum of plane waves approach in the scalar approximation [14,15,17]. A 2D Fourier transform is first applied to the converging beam in the plane just

#140190 - $15.00 USD Received 4 Jan 2011; revised 13 Apr 2011; accepted 14 Apr 2011; published 25 Apr 2011
(C) 2011 OSA

behind the PRP. The angular spectrum of plane waves is thus obtained. The latter is then propagated up to the focusing plane by applying the appropriate phase changes. Finally, an inverse 2D Fourier transform is performed to obtain the desired PSF.

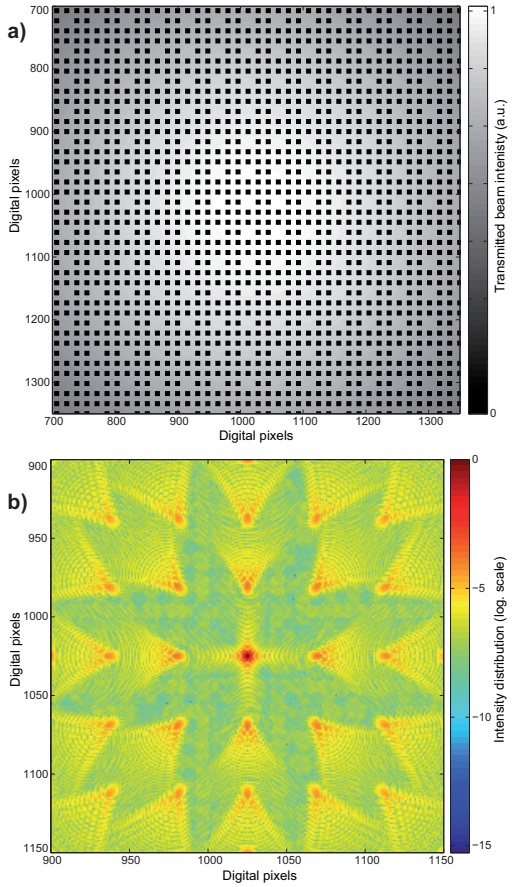

Fig. 3. PRP impact on PSF: (a) converging wave after PRP crossing; (b) computed PSF in the focusing plane in logarithmic scale.

Computations have been performed on digitally generated images of 2048×2048 pixels, with a sampling distance of $0.2\,\mu m$ that avoids aliasing, and for a wavelength of $0.45\,\mu m$. The PRP is made of square dots of $2\,\mu m \times 2\,\mu m$ with a period of $4\mu m$ as used experimentally. Different proportions of absent dots have been considered in order to evaluate the effect of this parameter on the light budget. In Fig. 3(a), only the central part of the converging wave is presented for an improved visualization of the PRP structure. Figure 3(b) presents a typical PSF obtained with a logarithmic scale. As can be expected, secondary focusing spots appear that are distributed along a square grid. These secondary lobes present two drawbacks. Firstly, the light energy diffracted in these lobes is lost for the central part of the PSF. The light budget is therefore decreased. Secondly, these secondary lobes may contribute to ghost images by returning the detector light coming from out of axis specimen points. It is thus of prime importance to reduce the power of these secondary lobes to the minimum in order to avoid these drawbacks. The width of the central lobe of the PSF is not affected by the PRP. This fact can be understood easily since the dot distribution does not modify the numerical aperture of the converging beam.

#140190 - $15.00 USD Received 4 Jan 2011; revised 13 Apr 2011; accepted 14 Apr 2011; published 25 Apr 2011
(C) 2011 OSA

Table 1. Percentage of Incident Light Power Concentrated in the Central Peak of the Diffraction Pattern in the Focus Plane Versus the Dot Material Transparency and the Proportion of Absent Dots

	Absent dots				
Dot Transparency	1/4	1/9	1/16	1/25	none
100% (no dot)	100%				
95%	98.1	97.7	97.6	97.6	97.5
75%	90.8	89.2	**88.6**	88.3	87.8
50%	82.2	79.1	78.0	77.5	76.6
25%	73.9	69.5	68.0	67.3	66.1
0%	66.0	60.5	**58.6**	57.8	56.3
0% - duty cycle: 0.4			**76.6**		

Computations were performed for different PRP configurations as summarized in Table 1. We observe that for completely opaque dots, the amount of light power concentrated in the central peak of the PSF is only 58.6% with a proportion of one absent dot out of every 16. After a double pass across the PRP, this would correspond to a light budget of only 34.2%. Such a drastic reduction of the light budget is not acceptable, especially in fluorescence microscopy that requires the minimizing of photobleaching. There are two main possibilities for reducing the rate of light loss due to the PRP. The first one is to use semi-transparent dots instead of opaque ones. One can see in the table that the amount of light intensity in the main PSF lobe increases with the dot transparency. A gain of 30%, from 58.6% to 88.6% is observed if the dot transparency is increased to 75%. Such a dot transparency would be easily detected by microscopy systems dedicated to biological samples that are known to produce relatively weak contrasts. A second way of reducing the impact of the PRP on the light budget is to decrease the pattern duty cycle by choosing a smaller dot size. In the last line of the table, with a duty cycle of 0.4; i.e. a dot size of $1.6\mu m$ instead of $2\mu m$, the percentage of light intensity concentrated in the central peak is increased from 58.6% to 76.6%. So, dot transparency and pattern duty cycle are two parameters that can be tuned for improving the overall light budget significantly. If a highly sensitive detection system is used, for instance with a photomultiplier tube in a confocal configuration, both dot transparency and duty cycle can be optimized to maintain the negligible light loss rate. If a less sensitive detection is used, proper imaging of the PRP may require light losses of up to 10% or 20%.

Ghost image formation is not an actual problem. In fact, the amount of light received by each secondary lobe is too small to contribute significantly to the detected image. This is especially true in an inverted configuration in which stray light has to be diffracted twice by the PRP. One may also notice than in fluorescence microscopy, since the diffraction pattern is wavelength dependent, the excitation PSF would be different from the emission one. This slight mismatch would still reduce the probability of stray light detection.

We would like to note that computations summarized in Table 1 have to be considered as orders of magnitude instead of sharp and definitive values since they correspond to specific setup parameters; for instance a numerical aperture of 0.5. For high numerical apertures, the scalar approximation is no longer valid and a vectorial approach is required [16]. Fluctuations of a few percent may thus be observed in the case of large numerical aperture lenses. In experiments presented in the following, we used PRPs produced in our technological facility. They present a dot transparency of about 40% and a duty cycle close to 0.4. They also present some

#140190 - $15.00 USD Received 4 Jan 2011; revised 13 Apr 2011; accepted 14 Apr 2011; published 25 Apr 2011
(C) 2011 OSA

dot shape irregularities and the overall light budget was evaluated to be 85% per PRP crossing.

3.3. *Positioning performances*

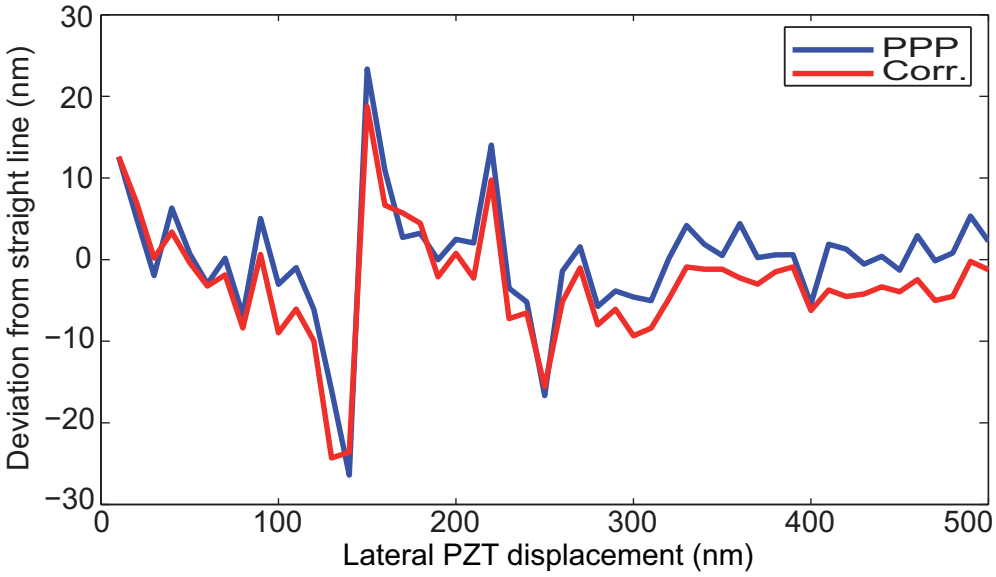

Fig. 4. Deviation of reconstructed PRP positions from a straight line for a linear displacement of 500 *nm* by the PZT. *blue:* PRP method; *red:* subpixel correlation method. Standard deviation between two curves: 2.5 *nm*

The method capabilities to provide absolute and high-accuracy in-plane coordinates of the fields of observation from the processing of the PRP images have been demonstrated elsewhere [13, 17, 18]. Resolutions achieved are in the range of a few nanometers for lateral position and of 10^{-3} degree for in-plane orientation. As an illustration, Fig. 4 presents the lateral positions reconstructed by the PRP method in comparison with that reconstructed from a typical image correlation method. In this experiment, the PRP is attached to a (PI P-615) servo-controlled piezoelectric translator (PZT) and observed by means of a $10\times$ magnification objective and a 56 *dB* CCD camera. The PZT was then shifted by steps of 10 *nm* over a distance of 500 *nm* with the recording of an image at each position. This set of images has been processed following the PRP decoding procedure as well as by a subpixel correlation method used as a reference. After subtraction of the mean straight line we obtain the curves presented in Fig. 4. We can see that the two curves suffer from the same distortions, about 50 *nm* peak to peak. The latter are due to PZT behavior that is unable to achieve the required positions as well as to external mechanical disturbances. In spite of this non-linear PZT displacement, the distance between the two curves remains very small and its standard deviation is only 2.5 *nm*. From these data the lateral resolution of the PRP method can be estimated to be better than 10 *nm* by considering the usual 3σ interval [19].

These high accuracy capabilities have been used for the characterization of the performances of the motorized stage (Prio Scientific H117 ProScan) used in our microscopy setup. For this purpose, we chose a set of five reference positions, a few tens of micrometers apart from each other. Then we send a control signal to the stage to rejoin successively every position and to reproduce this cycle 25 times. At each stop, an image of the PRP was recorded and then processed in order to determine the positions actually visited by the motorized stage. Figures 5(a) and 5(b)

#140190 - $15.00 USD Received 4 Jan 2011; revised 13 Apr 2011; accepted 14 Apr 2011; published 25 Apr 2011
(C) 2011 OSA

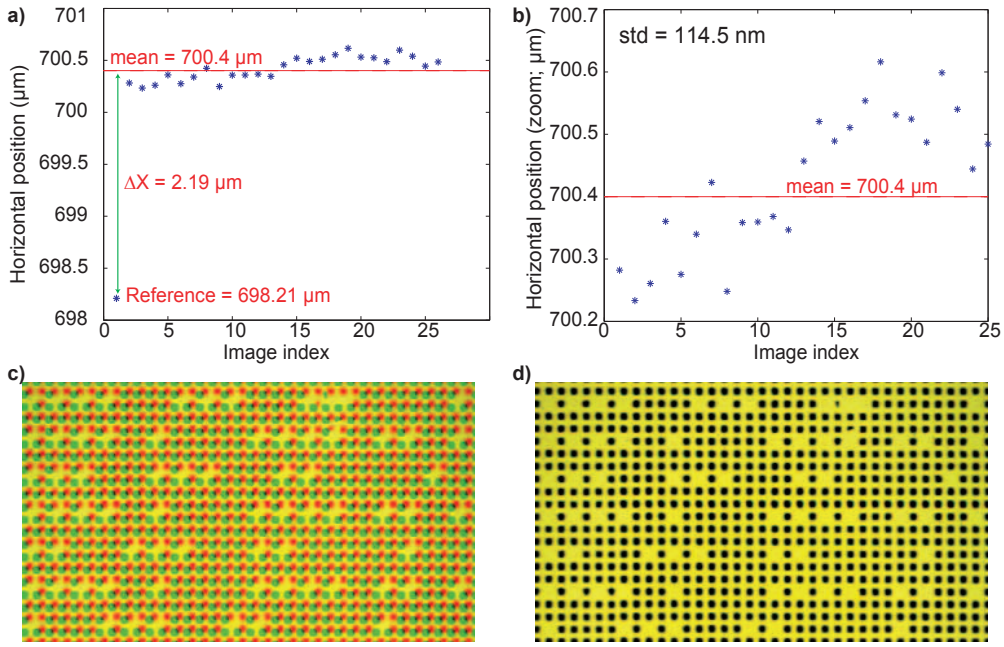

Fig. 5. Characterization of motorized microscope stage capabilities to retrieve a given position. (a) successive stage positions as reconstructed by PRP image processing. (b) same as (a) without reference position. (c) direct superimposition of reference image (red) with the second image (green). (d) same as (c) after image registration from PRP position.

present the results obtained for the first position. The latter are similar to that obtained for the other four reference positions. We can observe that despite quiet a good repeatability (Fig. 5(b)), the positions retrieved by the stage are at a distance of more than $2\mu m$ from the expected reference position (Fig. 5(a)). A systematic error thus appears quite clearly. It is significant and may be dependent on the stage motion history. If the image recorded at the reference position is directly superimposed on that recorded after the first cycle, as would be done by using standard video-microscopy methods, we obtain the result presented in Fig. 5(c). The effect of the systematic error appears clearly as severe blurring of the image obtained. However, if PRP data are used for digital subpixel image registration, we then obtain the superimposition shown in Fig. 5(d). In this case the systematic error is compensated for and images can be compared as if no stage displacements had occurred. This capability of PRM to comply with motorized stage limitations and to take them into account for sharp image registration is a second advantage in comparison with usual video-microscopy procedures.

4. Live cell application

4.1. Cell growth observation

PRM has been validated by observing the growth of a live cell culture by means of different microscopy modes. In this experiment, Pétri culture dishes are systematically transferred from the incubator to the microscope stage for every observation and vice-versa after the observation. The zone of interest is easily retrieved by means of PRP data. Furthermore, the highly accurate lateral coordinates obtained are used for image registration. We thus obtain a sequence of images displayed in a common reference system and in which the differences observed are only representative of transformations that have occurred in the cell culture. Figure 6 presents

#140190 - $15.00 USD Received 4 Jan 2011; revised 13 Apr 2011; accepted 14 Apr 2011; published 25 Apr 2011
(C) 2011 OSA

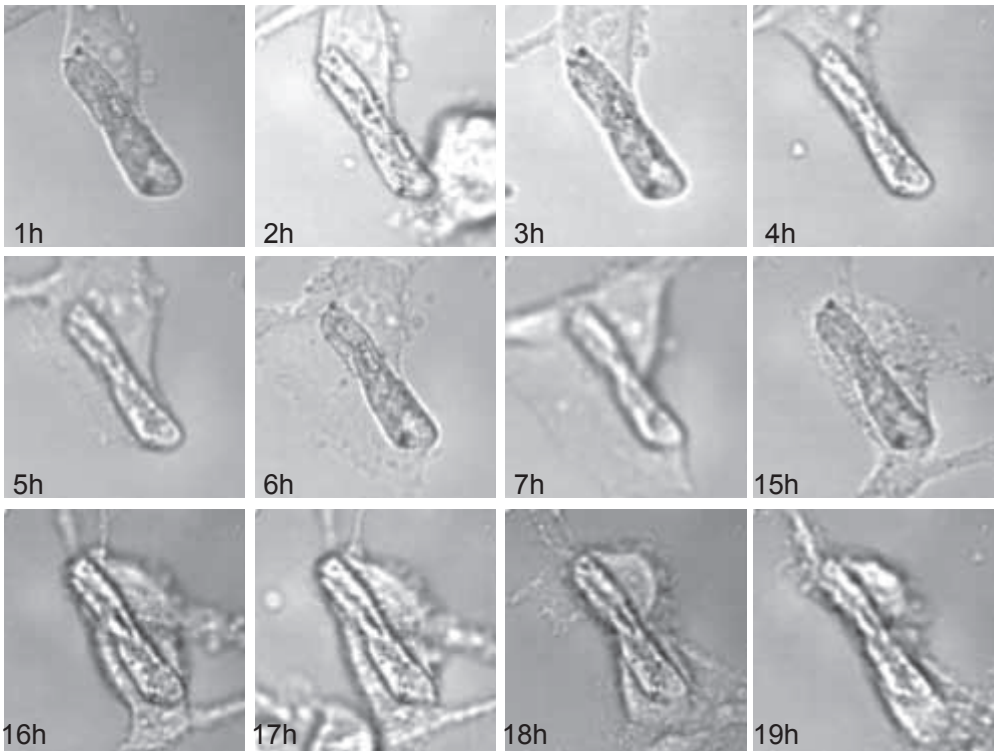

Fig. 6. Evolution of a fibroblast culture as observed by phase contrast microscopy. The chosen zone corresponds to a dust artefact around which cells are transforming. Sequence of images after digital registration by the PRM method. Image size: 120×120 pixels; $48 \times 48\,\mu m^2$; $60\times$ oil lens N.A.=1.42.

such a sequence of images as obtained from a human fibroblast culture observed at time intervals of one hour over two days by phase contrast microscopy. To illustrate PRM capabilities to retrieve a region of interest with high resolution, we made a zoom on a zone in which a dust artefact is stuck on the Pétri dish. This particle appears as a diagonal stick around which cells are proliferating. We can observe that the particle of interest lies at the same image location in all the images while cells take different forms and extensions. One may also notice that PRM is only concerned with lateral positions and remains insensitive to focus adjustments or light intensity fluctuations.

A different zone of that fibroblast culture is presented in the video of Fig. 7 that was obtained by fluorescence confocal microscopy on the same setup. In this case, a CFDA-SE fluorochrom is used for labeling membrane and intracellular proteins of fibroblast cells. The video demonstrates again the ability of PRM to comply with cell culture transfers from cell incubator to microscope stage and to provide high resolution image registrations suitable for live cell culture monitoring.

4.2. Internalization of apoptotic bodies by fibroblasts

Apoptosis is a highly regulated process of cell death and plays a fundamental role in the maintenance of tissue homeostasis in adult organisms. Numerous studies in recent years have revealed that apoptosis is a constitutive suicide programme expressed in most, if not all cells, and can be triggered by a variety of extrinsic and intrinsic signals.

#140190 - $15.00 USD Received 4 Jan 2011; revised 13 Apr 2011; accepted 14 Apr 2011; published 25 Apr 2011
(C) 2011 OSA

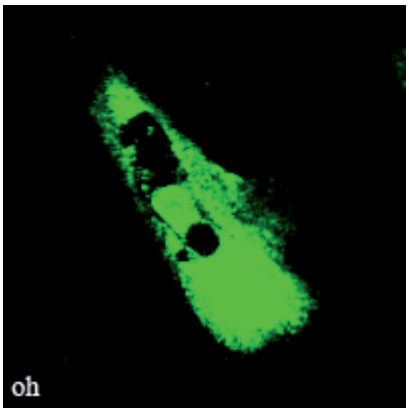

Fig. 7. (Media 1) Video of a fibroblast cell as observed by fluorescence confocal microscopy and after image registration by PRM. Image size: 200×200 pixels; $120 \times 120\,\mu m^2$; $20\times$ dry N.A.=0.5.

During the cell death process, the cell undergoes nuclear and cytoplasmic condensation with blebbing of the plasma membrane, and eventually breaks up into membrane-enclosed particles termed apoptotic bodies containing intact organelles, as well as portions of the nucleus. These apoptotic bodies are then rapidly recognized, ingested and degraded by specified phagocytes or neighboring cells [20].

Nonetheless, many studies have suggested that DNA from apoptotic bodies may even be rescued and reused by other cells, in which case we talk about horizontal DNA transfer. In the case that the transferred DNA harbors oncogenes, the recipient cell may become an immortal and transformed cell (cancerous cell).

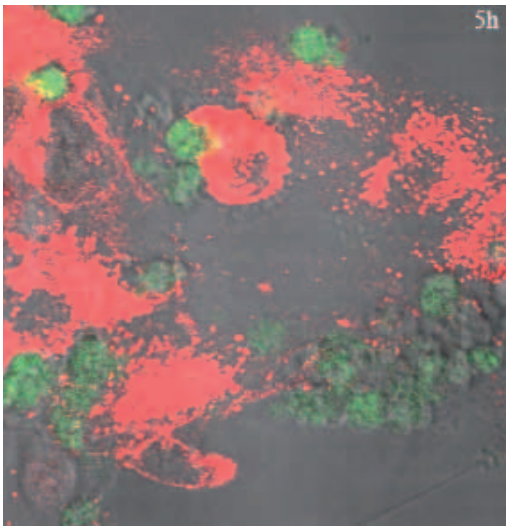

Fig. 8. (Media 2, Media 3) Video of the phagocytosis of an apoptotic body (green) by a fibroblast (red) as observed by fluorescence confocal microscopy and after image registration by PRM. Image size: 290×280 pixels; $116 \times 112\,\mu m^2$; $60\times$ oil N.A.=1.42.

Based on these observations, biologists are investigating if this phenomena is also applica-

#140190 - $15.00 USD Received 4 Jan 2011; revised 13 Apr 2011; accepted 14 Apr 2011; published 25 Apr 2011
(C) 2011 OSA

ble to cervical cancer cells, which is a cancer induced by oncogenic human papillomaviruses [21, 22]. To corroborate this, we used encoded Pétri dishes for monitoring in a same cell the dynamics of apoptotic body internalization by healthy cells. For this purpose, we tracked the cellular evolution of a co-culture of human fibroblast cells with apoptotic bodies. Fibroblast cytoskeleton was labeled with a red dye (PKH26) while in a separate culture dish, apoptotic bodies where labeled with a green dye (CFDA-SE). Then apoptotic bodies were incubated with the fibroblasts for a 24 hours experiment of co-culture with an observation every hour by using the PRM technique. Different sites of interest were documented among which we could observe apoptotic body internalization by a fibroblast cell. The corresponding sequence of images is presented in the video of Fig. 8. This video combines images from confocal fluorescence microscopy of the two dyes with those obtained by phase contrast imaging. We observe significant displacements of the fibroblasts on the Pétri culture dish surface. We can see that all of the apoptotic body (green) adherent to a fibroblast (red) in the upper left part of the first image is progressively internalized within the fibroblast. The appearance of the yellow shade results from red-green combination at the same location. Discussion on the biological significance of this observation is outside the frame of this paper. The important thing here is the new possibility offered by PRM to reconstruct such videos from images registered digitally in a common reference system while obtained after multiple Pétri culture dish transfers from cell incubator to microscope stage.

5. Conclusions

This paper establishes what we call Position-Referenced Microscopy (PRM) as a mature technique for live cell culture monitoring by using various modes of optical microscopy. Proof of principle had been demonstrated previously on a biological specimen fixed on a microscope slide [12]. As described here, smart Pétri culture dishes inserting a PRP allow actual use of the technique in live cell experiments. The size of the encoded area has been extended to $1\,cm^2$ and the impact of the PRP on the light budget has been evaluated and discussed.

Biological observations allowed by PRM were already possible by monopolizing a video-microscopy equipment. The interest of the method is of practical order since culture dish transfers from microscope stage to cell incubator and vice-versa are now supported without performance deteriorations. Furthermore lateral resolution achieved by PRM is shown to be much better than that proposed by a motorized microscope stage. Unperfect stage displacements are quantified and compensated for with accurate image registration. Finally, live cell culture experiments reported in the paper, especially the internalization of an apoptotic body by a fibroblast, demonstrate the interest of PRM as a useful tool for biomedical research.

Acknowledgments

The authors acknowledge the Région de Franche-Comté for project funding and for supporting E. Gaiffe's PhD. J.A. Galeano Z. acknowledges the Institut National du Cancer (INCa) for PhD funding.

#140190 - $15.00 USD Received 4 Jan 2011; revised 13 Apr 2011; accepted 14 Apr 2011; published 25 Apr 2011
(C) 2011 OSA